THE JOURNAL OF PHYSICAL CHEMISTRY B

Article

pubs.acs.org/JPCB

Dynamics and Binding Affinity of Spin-Labeled Stearic Acids in β-Lactoglobulin: Evidences from EPR Spectroscopy and Molecular Dynamics Simulation

Rita Guzzi,*[,†,‡] Bruno Rizzuti,[§] and Rosa Bartucci[†,‡]

[†]Department of Physics, [‡]Unità CNISM, and [§]CNR-IPCF UoS Cosenza, LICRYL, and CEMIF.CAL, University of Calabria, Ponte P. Bucci 31C, 87036 Rende (CS), Italy

ABSTRACT: β-Lactoglobulin (β-LG) is a member of the lipocalin protein family involved in the transport of fatty acids and other small hydrophobic molecules. The main binding site is at a central cavity, referred to as "calyx", formed by the protein β-barrel sandwich. Continuous-wave and pulsed Fourier transform electron spin resonance (cw- and FT-EPR) spectroscopy and molecular dynamics (MD) simulation were combined to investigate the interaction of fatty acids with bovine β-LG. Stearic acid bearing the nitroxide label at different positions, *n*, along the acyl chain (*n*-SASL, *n* = 5, 7, 10, 12, 16) were used. The EPR data show that the protein affinity for SASL decreases on going from *n* = 5 to 16. This behavior is due to the accommodation of the SASL in the protein calyx, which is hampered by steric hindrance of the doxyl ring for $n \geq 10$, as evidenced by MD data. Conformation and dynamics of 5-SASL are similar to those of the unlabeled stearate molecule. 5-SASL in the protein binding site undergoes librational motion of small amplitude on the nanosecond time scale at cryogenic temperature and rotational dynamics with correlation time of 4.2 ns at physiological temperature. The results highlight the dynamical features of fatty acids/β-LG interaction.

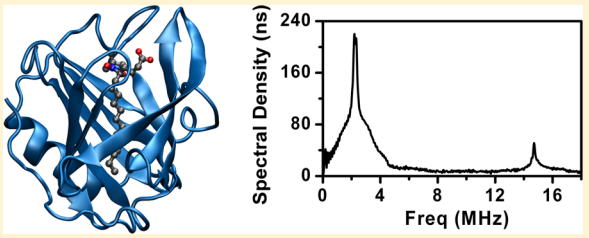

INTRODUCTION

β-Lactoglobulin (β-LG) is the most abundant protein in the milk of cows and many other mammalians, not including humans. Bovine β-LG is a relatively small lipocalin (162 residues, 18.3 kDa) involved in the binding and transport of hydrophobic and amphiphilic molecules such as fatty acids and retinoids. It is characterized by nine β-strands and a three-turn α-helix. Eight out of the nine β-strands are antiparallel and form a β-barrel sandwich with a central cavity, usually referred to as "calyx", which constitutes the main binding site of the protein.[1,2] The calyx is closed at one side and has the flexible loop 85−90 at the opposite side. Above a pH value of ∼7, β-LG undergoes the so-called Tanford transition, consisting in a movement of the loop 85−90 that enables the access of a ligand to the calyx.[3]

There is crystallographic and spectroscopic evidence that β-LG binds fatty acids with short (8 carbon atoms) to long (20 carbon atoms) aliphatic chain, in an almost extended conformation, with the carboxylate group anchored at the calyx entrance and the methylene segments extending in the hydrophobic interior of the cavity.[4−8] The fatty acid affinity depends on the aliphatic chain length, the highest values being reported for palmitic (C16:0) and stearic acid (C18:0).[8−10] The high affinity for palmitic acid was explained in terms of the conformation of the binding site, which allows to maximize the interaction between the ligand polar head and the charged residues Lys69, Lys60, and Glu62. The same conformation is found for the stearic acid bound to β-LG, although the terminal methyl end of the chain is slightly bent at the bottom of the calyx due to the limited depth of the calyx.[8] Upon binding amphiphilic ligands, β-LG increases its stability against denaturation caused by heat,[11] urea,[12] and pressure.[13]

The binding process is regulated by hydrophobic and electrostatic interactions as well as by release of water molecules occurring when a fatty acid transfers from the aqueous phase to the binding cavity.[8] Solvent accessibility in a protein binding site is a topic of relevant interest in proteins and other biomolecular systems, as it largely contributes to determine the affinity and kinetics of association for a ligand. In this respect, β-LG is distinctive because the innermost part of its binding cavity appears to be not accessible to water molecules, as determined by nuclear magnetic resonance spectroscopy and molecular dynamics (MD) simulations.[14] In contrast, the outermost opening of the calyx is exposed to the solvent[7] and set to accept an incoming ligand. Another aspect to be considered in the protein/ligand complexes is their dynamical interaction, which is important for protein functioning. In this respect, the ligand mobility within the β-LG binding site is not yet fully addressed.

In the present work, we have investigated the dynamics and the binding affinity of stearic acids within the β-LG calyx by using continuous-wave electron paramagnetic resonance (cw-EPR) and pulsed spin echo EPR methods combined with MD simulations. We have used spin-labeled stearic acid bearing the doxyl ring with the paramagnetic −NO nitroxide moiety at different position, *n*, along the chain (*n*-SASL, *n* = 5, 7, 10, 12 and

Received: July 27, 2012
Revised: September 3, 2012
Published: September 5, 2012

dx.doi.org/10.1021/jp3074392 | *J. Phys. Chem. B* 2012, 116, 11608−11615

16). The overall results evidence a reduced affinity of stearic acids when n is stepped down the acyl chain because the −NO group is blocked at the entrance of the calyx due to steric hindrance. 5-SASL is well-accommodated in the binding site and accessible to the solvent. The dynamics of 5-SASL in the β-LG calyx is characterized by fast librational motions of small amplitude at low cryogenic temperature and by rotational dynamics on the nanosecond time scale at physiological temperature.

EXPERIMENTAL AND THEORETICAL METHODS

Materials. Bovine β-LG (type L-3908), deuterium oxide (99.9 atom % ^{2}H), and stearic acid spin labels, n-SASL (n-(4,4-dimethyloxazolidine-N-oxyl)stearic acid), were obtained from Sigma-Aldrich (St. Louis, MO). All materials were used as purchased with no further purification.

Sample Preparation. The samples used in each experiment were protein solutions spin-labeled with n-SASL prepared in D_2O. The pD of the protein solutions was 7.8. Protein concentration was determined spectrophotometrically using an extinction coefficient $\varepsilon_{278\ nm}$ = 17 600 M^{-1} cm^{-1}.[15] The required amount of n-SASL in ethanol stock solution was dried down in a glass vial by using a stream of nitrogen gas, and traces of residual solvent were removed under vacuum. A solution of β-LG in D_2O was added, and the spin-labeled fatty acid was taken up by incubation at room temperature with periodic mixing. For all of the samples the label concentration was 0.1 mM, and the protein/label molar ratio varied from 0.25 to 25.

EPR Spectroscopy. Continuous-wave cw-EPR spectra were recorded on an ESP-300 9-GHz spectrometer (Bruker, Karlsruhe, Germany) equipped with an ER4201 TE_{102} standard rectangular cavity and with an ER 411VT temperature controller (both from Bruker). For measurements at 77 K, the spin-labeled protein samples in quartz EPR tubes were rapidly frozen immediately before the measurements by plunging the tubes into a finger dewar containing liquid nitrogen. Spectra were recorded at 10 mW microwave power by using 100 kHz frequency field modulation.

Pulsed EPR data were collected on an ELEXSYS E580 9-GHz Fourier Transform FT-EPR spectrometer (Bruker, Karlsruhe, Germany) equipped with a MD5 dielectric resonator and a CF 935P cryostat (Oxford Instruments, U.K.). The spin-labeled protein samples in quartz EPR tubes (i.d. 4 mm) were rapidly frozen in liquid nitrogen and transferred in the resonant cavity that was pre-equilibrated at 77 K. The measurements were then carried out at increasing temperature.

Primary, two-pulse ($\pi/2-\tau-\pi-\tau-$echo) echo-detected (ED)-EPR spectra were obtained by recording the integrated spin−echo signal at fixed interpulse delay τ, while sweeping the magnetic field. The microwave pulse widths were 32 and 64 ns, with the microwave power adjusted to provide $\pi/2$ and π-pulses, respectively. The magnetic field was set to the EPR absorption maximum, and the integration window was 160 ns.

The original ED-spectra, $ED_T(2\tau,H)$, were corrected for instantaneous spin diffusion arising from static spin−spin interaction by using spectra recorded at 77 K, where motional contributions are negligible. The corrected spectra, $ED_T^{corr}(2\tau,H)$, recorded at temperature T are plotted as a function of magnetic field, H, according to ref 16

$$ED_T^{corr}(2\tau, H) = ED_T(2\tau, H)\frac{ED_{77K}(2\tau_0, H)}{ED_{77K}(2\tau, H)} \quad (1)$$

where τ_0 is the shortest value of τ, for which ED-spectra were obtained.

Relaxation rates, $W(H,\tau_1,\tau_2)$, were determined from the ratio of corrected ED spectra recorded at two different values, τ_1 and τ_2, of the interpulse delay by using the following relation[17]

$$W(H, \tau_1, \tau_2) = \ln\left[\frac{ED(2\tau_1, H)}{ED(2\tau_2, H)}\right]\cdot\frac{1}{2(\tau_2 - \tau_1)} \quad (2)$$

where $ED(2\tau,H)$ is the ED-spectral lineheight at field position H.

To obtain electron spin echo envelope modulation (ESEEM) spectra, three-pulse, stimulated echo ($\pi/2-\tau-\pi/2-T-\pi/2-\tau-$echo) decays were collected by using microwave pulse widths of 12 ns, with the microwave power adjusted to give $\pi/2$ pulses. The time delay T between the second and the third pulses was incremented from 20 ns by 700 steps of ΔT = 12 ns while maintaining the separation τ between the first and the second pulses constant at 168 ns. The magnetic field was set to the maximum of the EPR absorption, and a four-step phase-cycling program was used to eliminate unwanted echoes. The time-dependent echo amplitudes, $V(\tau,T)$, were processed to yield standardized ESEEM intensities, according to a protocol previously developed.[18,19]

Molecular Modeling and Dynamic Simulation. The topology of the stearate molecule was derived from the side chain of glutamate in the force-field GROMOS,[20] as previously described for palmitate.[21] The additional doxyl group was parametrized by following the procedure of Garay and Rodrigues.[22] Their model, originally developed for the GROMOS 43a2x force field,[23] has also been updated for the 53a6 version by using atomtypes NR, OA, and CH2r for the N, O, and CH_2 atoms in the doxyl ring, respectively, together with the corresponding revised parameters for bonded and van der Waals interactions.[20] Partial charges do not differ appreciably from those previously obtained,[22] which, in turn, are comparable to the ones for similar nitroxyde-containing adducts in the AMBER[24] and OPLS[25] force fields. The starting configuration for the doxyl group was built by using the PRODRG server,[26] further relaxed by energy minimization and attached to the stearate chain for each position to obtain n-SASL (n = 5, 7, 10, 12, and 16) with either chirality.

The structure of β-LG was obtained from the 3UEX entry of the Protein Data Bank,[8] containing the X-ray structure of the protein complexed with a stearic acid molecule within the calyx. Three missing residues in a disordered loop were reconstructed in silico by using the native protein as reference.[7] In the starting position, the 5-SASL was placed with its first 6 C atoms (C^1-C^6) extending from the binding site in all-trans conformation and its last 12 C atoms (C^7-C^{18}) in the same position as the corresponding atoms in the crystallographic structure of the stearic acid. Similarly, any other n-SASL molecules were placed in the calyx with its first n + 1 C atoms in all-trans conformation protruding from the calyx and the remaining C atoms in the same position as atoms C^7-C^{23-n} of the stearic acid in crystallography.

Simulations were carried out by using the GROMACS package.[27] The ionization state of all of the protein residues and of the fatty acid headgroup was set to be consistent with neutral pH, and 9 Na^+ counterions were added to obtain a null overall charge for the system. The protein−stearate complex was solvated in SPC water molecules[28] within a rhombic dodecahedron box with a minimum distance of 1 nm from any edge, and periodic boundary conditions were applied. The particle-mesh Ewald (PME) method was used for computing

dx.doi.org/10.1021/jp3074392 | J. Phys. Chem. B 2012, 116, 11608−11615

long-range electrostatic interactions.[29,30] Sampling was performed in the NPT ensemble by using a Berendsen barostat[31] and a velocity rescaling thermostat[32] with reference values of 10^5 Pa and 300 K, respectively. A time step of 2 fs was used for the integration of the equations of motion, and covalent bonds were constrained by using the P-LINCS algorithm.[33] After energy minimization, the temperature of the system was increased from 250 K over 0.1 ns. Production runs of 50 ns were performed for each *n*-SASL in both chirality after 5 ns of equilibration.

RESULTS AND DISCUSSION

Binding Affinity and Dynamics of *n*-SASL Complexed with *β*-LG. Cw-EPR spectra at 293 K of 5-SASL in *β*-LG solution at different protein/label molar ratios are reported in Figure 1.

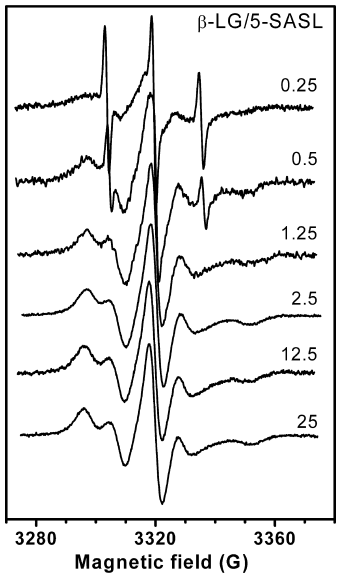

Figure 1. Cw-EPR spectra at 293 K of 5-SASL (0.1 mM) at increasing *β*-LG/label molar ratio in aqueous solution.

The label concentration is fixed (0.1 mM), and the spectra are recorded at increasing protein concentration (from 0.025 to 2.5 mM). Experiments at increasing protein concentration aim to minimize the interaction with fatty acid molecules at weak aspecific binding sites. The spectra at low protein concentration clearly show two components with different spectral anisotropy. In fact, an inner isotropic component contributed by free unbound labels is superimposed to an outer and more anisotropic signal due to a spin label population bound to the protein. The intensity of the mobile component of unbounded spin labels undergoing fast motion on the conventional EPR time scale disappears at increasing protein concentration. Single-component EPR spectra of bonded immobilized spin labels are obtained for *β*-LG/5-SASL molar ratio >1.25. The results indicate that the affinity of 5-SASL to *β*-LG increases with the protein concentration.

The binding affinity of spin-labeled stearic acids upon incubation with *β*-LG depends not only on protein concentration but also on the position, *n*, of the doxyl ring along the acyl chain. As it can be seen in Figure 2, the EPR spectra at 293 K of *n*-SASL in *β*-LG at protein/label molar ratio of 2.5 show some degree of immobilization when complexed with *β*-LG. However, the intensity of the sharp signal from unbound stearates increases from *n* = 10 position of label onward.

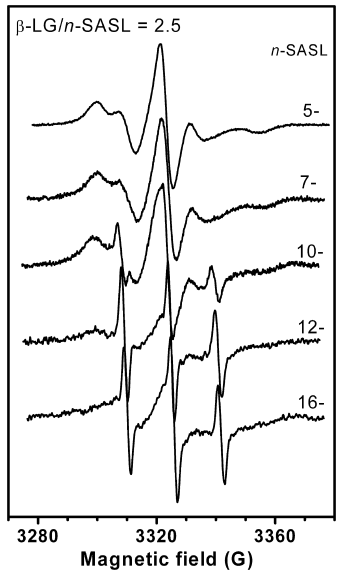

Figure 2. Cw-EPR spectra at 293 K of *n*-SASL bound to *β*-LG in aqueous solution. Protein/label molar ratio = 2.5.

The more *n* is stepped down along the chain, the more the affinity decreases, and higher protein concentration is required to approach the single-component anisotropic spectra. A considerable weaker affinity for *β*-LG of 12- and 16-SASL with respect to 5-SASL has been also reported in a previous study;[34] similarly, it was found that the affinity increases when the protein concentration is two-fold excess.

A useful spectral parameter for characterizing the dynamics of biomolecules under all conditions of immobilization is the outer hyperfine splitting in the EPR spectrum, $2\langle A_{zz}\rangle$, that is, the separation between the low-field maximum and the high-field minimum. It depends on both the amplitude (i.e., order) and rate of motion.[35,36] Large $2\langle A_{zz}\rangle$ values reflect a high degree of spin-label immobilization.

The $2\langle A_{zz}\rangle$ values of *n*-SASL in *β*-LG change as a function of *n* in the order: 5 < 7 < 10 < 12. Determination of $2\langle A_{zz}\rangle$ for 16-SASL was possible at higher protein concentration, and it results similar to that of 5-SASL. (See Table 1.)

Table 1. Separation of Outer Extrema in the cw-EPR Spectra of *n*-SASL Bound to *β*-LG in D_2O Solution at the Protein/Label Ratio of 2.5 or 7.5

n-SASL	$2\langle A_{zz}\rangle$ at 293 K (G)	$2A_{zz}$ at 77 K (G)	$\langle A_{zz}\rangle/A_{zz}$
5	54.8	69.8	0.78
7	56.8	69.1	0.82
10	57.6	68.0	0.85
12	58.6	67.4	0.87
16	54.9[a]	67.8[a]	0.81

[a]Protein/label ratio of 7.5.

Cw-EPR measurements on the same samples were also carried out in the frozen state at 77 K to determine the rigid limit values, $2A_{zz}$, of the outer hyperfine splittings. $2A_{zz}$ is a polarity-sensitive spectral parameter: an increase in environmental polarity leads to an increase in $2A_{zz}$.[35−37] As it can be seen in Table 1, $2A_{zz}$ values decrease progressively from *n* = 5 to 12 position of labeling, and an increase is seen at the *n* = 16 position. The results, therefore, correspond to a lower polarity around the spin-label environment on moving along the chain of the stearic acid up to the *n* =

dx.doi.org/10.1021/jp3074392 | J. Phys. Chem. B 2012, 116, 11608−11615

12 position and to a slight increase at the terminal methyl end (n = 16). The ratio between $2<A_{zz}>$ and $2A_{zz}$ allows us to compare the effects of motional averaging on the n-SASL spectra at 293 K, excluding the polarity dependence.[38] When motion is suppressed, the ratio is 1. The $<A_{zz}>/A_{zz}$ values show a maximum at n = 12 position (Table 1) and indicate that the mobility of the bound spin label is higher when the nitroxide ring is at either end of the chain. The rotational correlation time, τ_R, was calculated according to the following equation[35,36]

$$\tau_R = a(1 - S)^b \quad (3)$$

where a = 0.54 ns, b = −1.36, and $S = <A_{zz}>/A_{zz}$.

The values obtained are 4.2 ns for 5-SASL and 8.6 ns for 12-SASL, indicating a higher mobility of the 5-SASL in the β-LG binding site. These τ_R values are lower than those found for the 5- and 12-SASL bound to other fatty acid binding proteins such as lipoxygenase[38] (6.5 and 12.4 ns, respectively) or bovine serum albumin[39] (30 ns for both positions). The difference may be related to the differences in the structure of the ligand binding sites in these proteins. In addition, tear lipocalins/spin-labeled fatty acids complexes have a shorter correlation time than the protein alone, indicating that the ligands are not rigidly anchored in the cavity but move within the pocket.[40]

Interaction Model of *n*-SASL with β-LG. ESEEM spectroscopy in the time and frequency domain is widely used for determination of solvent accessibility to specific biosystem regions.[41−43]

Figure 3A shows the absolute-value ESEEM spectrum of 5-SASL/β-LG in D_2O solution at the protein/label molar ratio of 2.5.

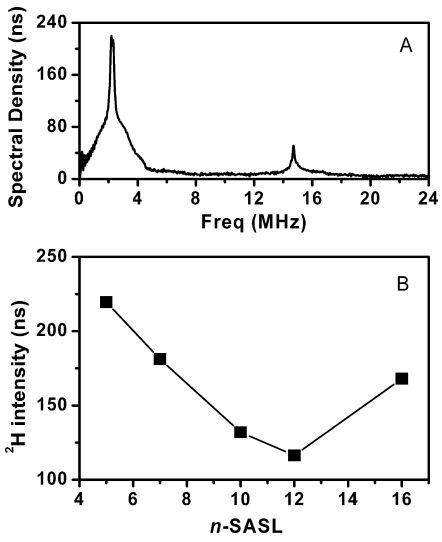

Figure 3. (A) Fourier-transform ESEEM spectrum at 77 K of 5-SASL bound to β-LG in D_2O solvent. (B) ^{2}H-ESEEM intensity for n-SASL in β-LG at 77 K. Protein/label molar ratio = 2.5.

The spectrum consists of a signal at the deuterium ^{2}H-Larmor frequency of ca. 2.2 MHz and another one at the proton ^{1}H-Larmor frequency of 14.5 MHz that arises from matrix protons. The ^{2}H peak of the spectrum, that specifically arises from D_2O in the proximity of the −NO spin label group, consists of a narrow doublet superimposed to a broad component. The narrow component corresponds to D_2O molecules that are not hydrogen-bonded to the spin-label group, whereas the broad component corresponds to D_2O molecules that are hydrogen-bonded to the nitroxide spin-label group.[18] Similarly, as for 5-SASL, ESEEM spectra were recorded for all n-SASL in β-LG at the protein/label molar ratio of 2.5. For any positions, the ^{2}H peak still consists of both a broad and sharp component (data not shown).

The dependence of the standardized intensities (i.e., the sum of the sharp and broad components) on the chain segment position, n, of the bound fatty acids is given in Figure 3B. This parameter directly reports on the accessibility of solvent (D_2O) to the spin-label moiety. The ^{2}H-ESEEM intensities decrease progressively up to a minimum value at n = 12 position and then increase when the nitroxide is located at the methyl end, similarly to the cw-EPR results at 77 K. (See $2A_{zz}$ in Table 1.) The trend of the profile in Figure 3B does not depend significantly on the protein/label molar ratio (data not shown).

The ^{2}H intensity shows relatively high values, compatible with a solvent accessible site for the spin label, as found for n-SASL in human serum albumin[44] and for cysteine-labeled residues located in the cytoplasmatic region of Na,K-ATPase.[45,46] This finding is quite unexpected because it has been previously reported that the β-LG cavity is a dry ligand-binding site both in the apo form and in the palmitate complexed one.[14]

To clarify this point and to gain insight into the atomic details of the protein/ligand interaction, we have performed MD simulations on the β-LG/stearic acid complex, with the fatty acid either in the native form or bearing the doxyl moiety at all five different n positions (n = 5, 7, 10, 12, 16) of the methylene chain. The fatty acid molecule without the doxyl ring was placed either in the crystallographic position or partially removed from the binding site, with its aliphatic chain shifted up to 10 methylene groups upward and the portion exposed to the solvent modeled in all-trans configuration. In any case, the stearate enters rapidly into the calyx, shifting the tail as deep as possible and remaining on average in an almost fully extended conformation.

Figure 4 shows the β-LG binding site containing representative simulation structures close to the average structures of stearic acid (A) without doxyl and with the doxyl ring at the (B) n = 5 and (C) 12 position of labeling.

In the presence of the spin label, the simulation data clearly show that the accommodation of the fatty acids within the binding site depends on the position of the doxyl ring along the hydrophobic chain. In fact, both 5- and 7-SASL penetrate completely into the calyx, whereas when the doxyl is bound to the other positions (i.e., 10-, 12-, and 16-SASL), the steric hindrance of the ring inhibits a complete penetration for the upper part of the lipid molecule. The doxyl ring is blocked always at the same position, with the nitroxide group −NO interacting with the loop 85−90 that is involved in the Tanford transition[3] and the opposite side mostly with the three hydrophobic residues in the loop 38−41 (i.e., Pro38, Leu39, and Val41) (Figure 4). The portion of the fatty acid chain above the ring does not extend into the solvent but tends to fold in a sort of hydrophobic collapse. The resulting conformation allows to avoid contact of the methylene groups with the water molecules and favors electrostatic interactions of the carboxylate head with nearby polar protein groups. This behavior is especially evident for the doxyl ring in position n = 10 and 12, for which the upper portion of the lipid chain largely hinders the dynamics of the spin label and shields it from the solvent. In the case of 16-SASL, the portion of the tail entering the binding cavity is so short that it has little anchoring effect for the molecule. The fatty acid occasionally starts to diffuse away into the solvent but it is pushed back into the calyx by the hydrophobic interactions. As a

dx.doi.org/10.1021/jp3074392 | J. Phys. Chem. B 2012, 116, 11608−11615

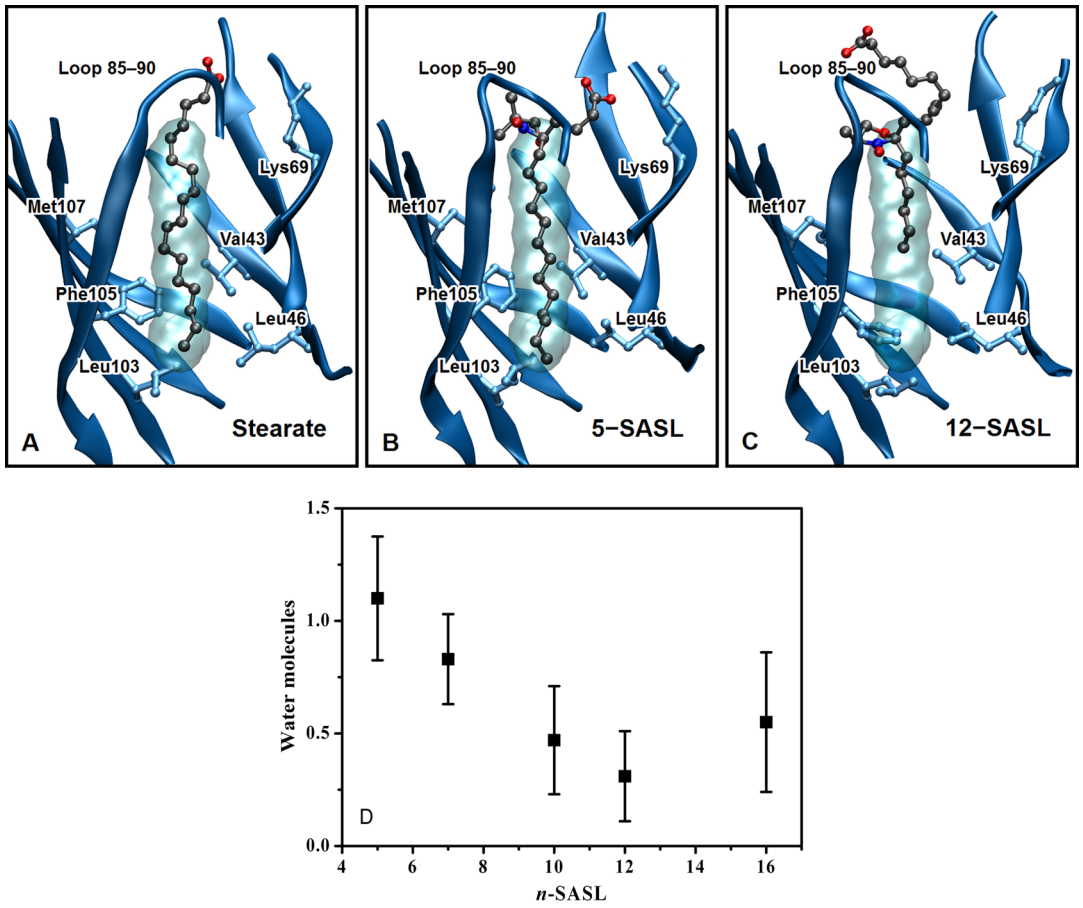

Figure 4. Comparison in simulation of different stearic acid molecules in the binding site of β-LG: (A) unlabeled fatty acid, (B) 5-SASL, and (C) 12-SASL. The transparent surface represents the cavity occupied by the C^5–C^{18} atoms of the fatty acid in the crystallographic structure;[8] selected protein residues are also shown. (D) Number of water molecules in contact with the −NO group of 5-SASL in simulation; cutoff distance is 0.35 nm.

consequence, 16-SASL is more exposed to the solvent compared with 10- and 12-SASL and also more mobile, in agreement with the cw-EPR data.

The localization of the doxyl ring at the entrance of the binding site determines the overall trend of its solvent accessibility. In fact, Figure 4D shows the average number of water molecules in contact with the −NO group during the simulation as a function of the position, n, of the doxyl ring along the fatty acid chain. As it can be observed, the water concentration progressively decreases as a function of n, except in correspondence of $n = 16$. This trend closely mirrors the polarity profile deduced from cw- and pulsed FT-EPR techniques, respectively. (See Table 1 and Figure 3B.) Steric hindrance was already hypothesized by Berliner et al.[34] to explain their ESR and fluorescence data relative to the interaction of 12- or 16-SASL with β-LG. The combination of experimental and computational data obtained here for all n-SASL acids gives a clear demonstration of the reduced binding affinity on moving the spin label down the hydrophobic chain.

In Figure 5, the simulated root-mean-square fluctuations (RMSFs) of the atomic position of the C atoms for stearic acid and for the five different spin-labeled n-SASL complexed with β-LG are compared.

The data indicate that the presence of the doxyl ring at $n = 5$ position does not alter considerably the flexibility of the fatty acid chain. The maximum difference of flexibility for 5-SASL with respect to the native fatty acid is found in correspondence of the C^5 atom, where the doxyl is attached. This difference, $\Delta RMSF_{max} \approx 0.03$ nm, is within the statistical uncertainty associated with the

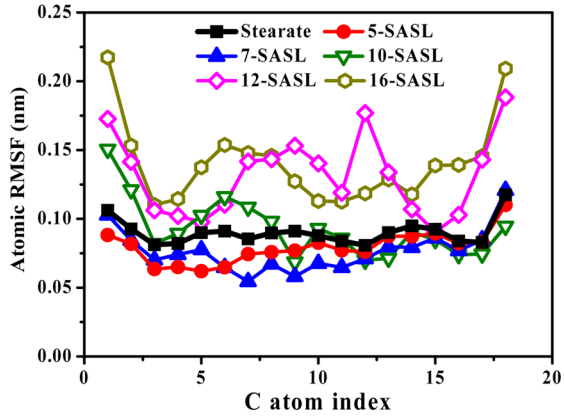

Figure 5. Simulated root-mean-square fluctuations (RMSFs) of the atomic position of the C atoms along the chain for unlabeled stearic acid and for the five different stearic acid spin-labels, n-SASL, bound to β-LG. The uncertainty is 0.02 nm.

two curves. Similar fluctuations are found for 7-SASL, although in this case a systematic discrepancy in correspondence of the doxyl position at C^7 atom is more evident. All other spin-labeled stearic molecules ($n \geq 10$) show a flexibility profile that is distinctively different from the one of the unlabeled fatty acid.

Overall, by comparing the structural data obtained from MD simulation of β-LG and fatty acid with and without doxyl ring at the $n = 5$ position, it is evident that both the dynamics and

dx.doi.org/10.1021/jp3074392 | J. Phys. Chem. B 2012, 116, 11608–11615

structure of the stearate are not significantly affected by the presence of the spin label in this position. Regardless of the presence of the doxyl group, the aliphatic chain is extended into the binding site and interacts with the same protein residues, which include Ile56 and Val92, the ring of the two Phe residues 82 and 105, and the side chains of three Leu residues 46, 54, and 103. (See Figure 4A,B.) In particular, the ring of Phe105 is always approximately parallel to both native stearic acid and 5-SASL, whereas for $n \geq 10$ it occupies the space left empty by the fatty acid chain and lies perpendicular and below it. (See Figure 4C.) In addition, compared with the other spin-labeled fatty acids, the position of 5-SASL is more conveniently stabilized by electrostatic interactions with Lys69 and Lys60, anchoring the negatively charged headgroup. The simulated dynamics of all of the β-LG residues above-mentioned is similar in the presence of 5-SASL and unlabeled fatty acid, as indicated by positional RMSF of both main-chain and side-chain atoms (data not shown).

Therefore, 5-SASL represents a suitable probe to determine both the dynamics and the solvent accessibility of the fatty acid in the β-LG binding site.

Librational Motion of the 5-SASL/β-LG Complex. Two-pulse, ED-EPR spectroscopy is particularly appropriate to study the dynamics of spin-labeled biosystems in the low-temperature regime.[41,47,48]

The dynamics of the 5-SASL bound to β-LG was investigated by ED-EPR spectra recorded in the 77−240 K temperature range. Figure 6A shows the ED-EPR spectra at 200 K recorded on increasing the echo delay time, τ, from 168 to 552 ns.

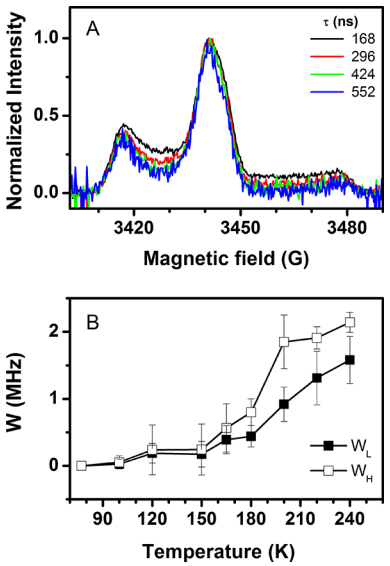

Figure 6. (A) Echo-detected EPR spectra at 200 K of 5-SASL/β-LG solution recorded at different interpulse separation. Spectra are corrected for instantaneous diffusion according to eq 1 and are normalized to the maximum line height. (B) Temperature dependence of W_L (open symbols) and W_H (solid symbols) relaxation rate parameters of 5-SASL/β-LG solution.

The spectra have been corrected for instantaneous spin diffusion according to eq 1 by using spectra recorded at 77 K, where little molecular motion is expected.[16] Moreover, they have been normalized to the central line to display only the field-dependent part of the relaxation. The dependence of the ED lineshapes on the τ-interpulse separation reveals preferential relaxation in the intermediate spectral regions at low- and high-field that is characteristic of rapid, small-amplitude libration.[47,49]

To characterize the librational motion of 5-SASL, we have evaluated the anisotropic curves of the relaxation rate, W, from the ED-EPR spectra according to eq 2 at each temperature (data not shown). They coincide within the noise level, showing that the relaxation is close to exponential. This is consistent with the so-called "isotropic" model for librational dynamics, in which uncorrelated librational motions take place simultaneously about the nitroxide x, y, and z axes.[16,17] The relaxation rates are characterized by the maximum values, W_L and W_H, determined in the low- and high-field regions, respectively, of the ED spectra.

Figure 6B shows the plots of both the W_L and the W_H values of 5-SASL in β-LG in the 77−240 K temperature range. The temperature profiles of W_L (open symbols) and W_H (solid symbols) are similar, showing consistency between the relaxation effects on the low- and high-field regions of the ED-EPR spectra. The difference between the W_L and W_H values arises simply from the different inherent sensitivities of the low- and high-field spectral regions to librational motion.[16,17] The plots indicate that the librational motion is activated starting from 100 K, then increases moderately up to ~180 K and more rapidly above this temperature.

Figure 7A shows the temperature dependence of the librational amplitude-correlation time product, $\langle\alpha^2\rangle\tau_c$, for the 5-SASL/$\beta$-LG complex.

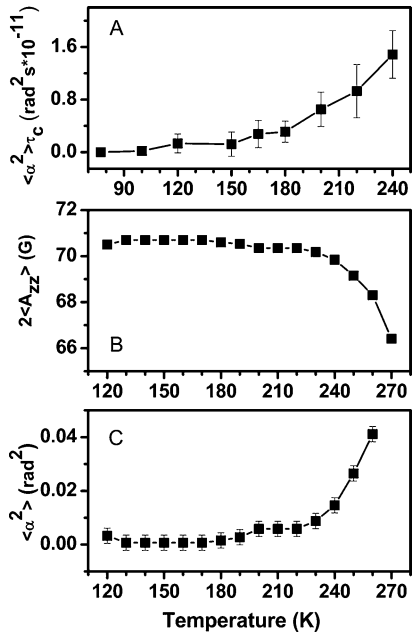

Figure 7. Temperature dependence of (A) amplitude-correlation time product, $\langle\alpha^2\rangle\tau_c$, (B) outer hyperfine splitting, $2\langle A_{zz}\rangle$, and (C) librational amplitude, $\langle\alpha^2\rangle$, of 5-SASL/β-LG solution in D_2O.

The $\langle\alpha^2\rangle\tau_c$ values are obtained from the W_L values that are given in Figure 6B by using a conversion factor relating $\langle\alpha^2\rangle\tau_c$ to W_L of 1.41×10^{17} rad^{-2} s^{-2}, as previously established both for phospholipids spin-labeled in the lipid chain and for alamethicin spin-labeled with TOAC, by using spectral simulations with the "isotropic" librational model.[17,50] The temperature profile of the amplitude-correlation time product, $\langle\alpha^2\rangle\tau_c$, mirrors that obtained for the relaxation rate, W. Indeed, $\langle\alpha^2\rangle\tau_c$ values remain very low up to 180 K and then gradually increase.

dx.doi.org/10.1021/jp3074392 | J. Phys. Chem. B 2012, 116, 11608−11615

To determine the mean-square amplitude, $\langle\alpha^2\rangle$, of the librational motion, we also recorded conventional cw-EPR spectra of 5-SASL/β-LG as a function of temperature (data not shown). Powder spectra with broad lines are obtained at low temperature, whereas from 220 K onward they narrow progressively and achieve an almost sharp lineshape at high temperature.

The temperature effects on the cw-EPR lineshapes of the ligand/protein complex can be derived from the temperature dependence of the outer hyperfine splittings, 2 $\langle A_{zz}\rangle$, that is given in Figure 7B. The values are approximately constant over a broad temperature range and above 220 K decrease with the temperature, as a result of both progressive motional narrowing by librations[51] and unfreezing of rotations of the label methyl groups.[52]

The temperature dependence of the mean-square amplitude, $\langle\alpha^2\rangle$, of the librational motion of 5-SASL in β-LG is given in Figure 7C. For small-amplitude fast libration, these values are derived from the following equation[51]

$$\langle A_{zz}\rangle = A_{zz} - (A_{zz} - A_{xx})\langle\alpha^2\rangle \quad (4)$$

where $\langle A_{zz}\rangle$ is the motionally averaged splitting of the hyperfine tensor of principal elements A_{xx}, A_{yy}, and A_{zz}.

The $\langle\alpha^2\rangle$ values start to increase from 200 K and more significantly from 230 K. The temperature dependence of $\langle\alpha^2\rangle$ is similar to that observed previously by cw- and pulsed EPR for small spin probes in glass-forming solvents,[53,54,56] for spin-labeled frozen lipid dispersions,[17,55] for chain-labeled stearic acids inserted in the binding sites of human serum albumin,[44] for spin-labeled Na,K-ATPase,[45] and for the photosynthetic bacterial reaction center.[57] The behavior of $\langle\alpha^2\rangle$ as a function of temperature is analogous to that of the mean-square atomic displacement, $\langle r^2\rangle$, determined by neutron scattering[59] and Mossbauer spectroscopy[58] and related to a dynamical transition observed in hydrated protein at $T \geq 200$ K.[59]

At the highest temperature, the root-mean-square amplitude of the librational motion is $7 \pm 1°$ and, by combining $\langle\alpha^2\rangle\tau_c$ with $\langle\alpha^2\rangle$ values, the librational correlation time of the ligand/protein complex is $\tau_c = 1.1 \pm 0.3$ ns. These librational parameters are comparable to those obtained, under the same experimental condition for Na,K-ATPase with[46] and without urea[45] and for the peptide TOAC-1 in lipid membranes.[50] Similar angular amplitude was found for spin-labeled stearic acids in albumin,[44] although τ_c was shorter. Finally, higher α values are found for spin-labeled hemoglobin[60] and for chain-labeled membranes,[17] with a librational correlation time in the subnanosecond regime (0.3 ns). The dynamics of 5-SASL bound to β-LG is slower compared with that in albumin, although it shows in both cases the same librational amplitude. This result may be due to the distinctive features of the three high-affinity binding sites of albumin, which are long and narrow hydrophobic pockets opened at both ends.[61]

CONCLUSIONS

EPR data and MD results allow us to gain molecular details of the interaction between chain labeled stearic acids, *n*-SASL, and β-LG. 5- (and 7-) SASL show the highest affinity for the protein. For $n \geq 10$ SASL, the presence of the doxyl ring hinders the complete insertion into the calyx. This is responsible for the reduced affinity and for the dynamical behavior and water penetration profiles of spin-labeled stearic acids bound to β-LG.

5-SASL optimally fits in β-LG calyx in a fully extended conformation. Its doxyl ring is located at the entrance of the cavity and is accessible to the solvent, with the nitroxide group interacting with the 85−90 flexible loop. The ligand dynamics is on the nanosecond time scale and shows librational and rotational features at cryogenic and physiological temperature, respectively.

The overall findings highlight the ability of β-LG to bind within its central cavity hydrophobic or amphiphilic molecules of appropriate length and size, which is relevant to β-LG function.

AUTHOR INFORMATION

Corresponding Author

*E-mail: rita.guzzi@fis.unical.it.

Notes

The authors declare no competing financial interest.

REFERENCES

(1) Kontopidis, G.; Holt, C.; Sawyer, L. *J. Mol. Biol.* **2002**, *318*, 1043−1055.
(2) Kontopidis, G.; Holt, C.; Sawyer, L. *J. Dairy Sci.* **2004**, *87*, 785−796.
(3) Qin, B. Y.; Bewley, M. C.; Creamer, L. K.; Baker, H. M.; Baker, E. N.; Jameson, G. B. *Biochemistry* **1998**, *37*, 14014−14023.
(4) Wu, S. Y.; Pérez, M. D.; Puyol, P.; Sawyer, L. *J. Biol. Chem.* **1999**, *274*, 170−174.
(5) Ragona, L.; Fogolari, F.; Zetta, L.; Perez, D. M.; Puyol, P.; De Kruif, K.; Lohr, F.; Ruterjans, H.; Molinari, H. *Protein Sci.* **2000**, *9*, 1347−1356.
(6) Collini, M.; D'Alfonso, L.; Molinari, H.; Ragona, L.; Catalano, M.; Baldini, G. *Protein Sci.* **2003**, *12*, 1596−1603.
(7) Loch, J. I.; Polit, A.; Gorecki, A.; Bonarek, P.; Kurpiewska, K.; Dziedzicka-Wasylewska, M.; Lewinski, K. *J. Mol. Recognit.* **2011**, *24*, 341−349.
(8) Loch, J. I.; Polit, A.; Bonarek, P.; Olszewska, D.; Kurpiewska, K.; Dziedzicka-Wasylewska, M.; Lewinski, K. *Int. J. Biol. Macromol.* **2012**, *50*, 1095−1102.
(9) Frapin, D.; Dufour, E.; Haertlé, T. *J. Protein Chem.* **1993**, *4*, 443−449.
(10) Liu, L.; Kitova, E. N.; Klassen, J. S. *J. Am. Soc. Mass Spectrom.* **2011**, *22*, 310−318.
(11) Barbiroli, A.; Bonomi, F.; Ferranti, P.; Fessas, D.; Nasi, A.; Rasmussen, P.; Iametti, S. *J. Agric. Food Chem.* **2011**, *59*, 5729−5737.
(12) Busti, P.; Scarpeci, S.; Gatti, C. A.; Delorenzi, N. J. *Food Hydrocolloids* **2005**, *19*, 249−255.
(13) Considine, T.; Patel, H. A.; Singh, H.; Creamer, L. K. *Food Chem.* **2007**, *102*, 1270−1280.
(14) Qvist, J.; Davidovic, M.; Hamelberg, D.; Halle, B. *Proc. Natl. Acad. Sci. U.S.A.* **2008**, *105*, 6296−6301.
(15) Dufour, E.; Roger, P.; Haertle, T. *J. Protein Chem.* **1992**, *11*, 645−652.
(16) Erilov, D. A.; Bartucci, R.; Guzzi, R.; Marsh, D.; Dzuba, S. A.; Sportelli, L. *J. Phys. Chem. B* **2004**, *108*, 4501−4507.
(17) Erilov, D. A.; Bartucci, R.; Guzzi, R.; Marsh, D.; Dzuba, S. A.; Sportelli, L. *Biophys. J.* **2004**, *87*, 3873−3881.
(18) Erilov, D. A.; Bartucci, R.; Guzzi., R.; Shubin, A. A.; Maryasov, A. G.; Marsh, D.; Dzuba, S. A.; Sportelli, L. *J. Phys. Chem. B* **2005**, *109*, 12003−12013.
(19) Bartucci, R.; Guzzi, R.; Sportelli, L.; Marsh, D. *Biophys. J.* **2009**, *96*, 997−1007.
(20) Oostenbrink, C.; Villa, A.; Mark, A. E.; van Gunsteren, W. F. *J. Comput. Chem.* **2004**, *25*, 1656−1676.
(21) Rizzuti, B.; Pantusa, M.; Guzzi, R. *Spectroscopy* **2010**, *24*, 159−163.
(22) Garay, A. S.; Rodrigues, D. E. *J. Phys. Chem. B* **2008**, *112*, 1657−1670.
(23) Berger, O.; Edholm, O.; Jahnig, F. *Biophys. J.* **1997**, *72*, 2002−2013.

(24) Improta, R.; Di Matteo, A.; Barone, V. *Theor. Chem. Acc.* **2000**, *104*, 273−279.
(25) Murzyn, K.; Rog, T.; Blicharski, W.; Dutka, M.; Pyka, J.; Szytula, S.; Froncisz, W. *Proteins* **2006**, *62*, 1088−1100.
(26) Schüttelkopf, A. W.; van Aalten, D. M. F. *Acta Crystallogr., D* **2004**, *60*, 1355−1363.
(27) Hess, B.; Kutzner, C.; van der Spoel, D.; Lindahl, E. *J. Chem. Theory Comput.* **2008**, *4*, 435−447.
(28) Berendsen, H. J. C.; Postma, J. P. M.; van Gunsteren, W. F.; Hermans, J. Interaction Models for Water in Relation to Protein Hydration. In *Intermolecular Forces*; Pullman, B. Ed.; Reidel: Dordrecht, The Netherlands, 1981; p 331.
(29) Darden, T.; York, D.; Pedersen, L. *J. Chem. Phys.* **1993**, *98*, 10089−10092.
(30) Essmann, U.; Perera, L.; Berkowitz, M. L.; Darden, T.; Lee, H.; Pedersen, L. G. *J. Chem. Phys.* **1995**, *10*, 8577−8593.
(31) Berendsen, H. J. C.; Postma, J. P. M.; Di Nola, A.; Haak, J. R. *J. Chem. Phys.* **1984**, *81*, 3684−3690.
(32) Bussi, G.; Donadio, D.; Parrinello, M. *J. Chem. Phys.* **2007**, *126*, 014101−014108.
(33) Hess, B. *J. Chem. Theory Comput.* **2008**, *4*, 116−122.
(34) Narayan, M.; Berliner, L. J. *Biochemistry* **1997**, *36*, 1906−1911.
(35) *Spin Labeling: Theory and Applications*; Berliner, L. J., Ed; Academic Press: New York, 1976; Vol. *I*.
(36) Marsh, D. Electron Spin Resonance: Spin-Labels. In *Membrane Spectroscopy: Molecular Biology, Biochemistry and Biophysics*; Grell, E., Ed.; Springer: Berlin, 1981; Vol. *31*, p 51.
(37) Klare, J. P.; Steinhoff, H. J. *Photosynth. Res.* **2009**, *2*−*3*, 377−390.
(38) Wu, F.; Gaffney, B. J. *Biochemistry* **2006**, 4512510−12518.
(39) Livshits, V. A.; Marsh, D. *Biochim. Biophys. Acta* **2000**, *1466*, 350−360.
(40) Glasgow, B. J.; Gasymov, O. K.; Abduragimov, A. R.; Yusifov, T. N.; Altenbach, C.; Hubbell, W. L. *Biochemistry* **1999**, *41*, 13707−13716.
(41) Bartucci, R.; Erilov, D.; Guzzi, R.; Sportelli, L.; Dzuba, S. A.; Marsh, D. *Chem. Phys. Lipids.* **2006**, *141*, 142−157.
(42) Volkov, A.; Dockter, C.; Bund, T.; Paulsen, H.; Jeschke, G. *Biophys. J.* **2009**, *96*, 1124−1141.
(43) Dikanov, S. A.; Tsvetkov, Y. D. *Electron Spin Echo Envelope Modulation (ESEEM) Spectroscopy*; CRC Press: Boca Raton, FL, 1992.
(44) De Simone, F.; Guzzi, R.; Sportelli, L.; Marsh, D.; Bartucci, R. *Biochim. Biophys. Acta* **2007**, *1768*, 1541−1549.
(45) Guzzi, R.; Bartucci, R.; Sportelli, L.; Esmann, M.; Marsh, D. *Biochemistry* **2009**, *48*, 8343−8354.
(46) Guzzi, R.; Babavali, M.; Bartucci, R.; Sportelli, L.; Esmann, M.; Marsh, D. *Biochim. Biophys. Acta, Biomembr.* **2011**, *1808*, 1618−1628.
(47) Dzuba, S. A.; Tsvetkov, Yu. D.; Maryasov, A. G. *Chem. Phys. Lett.* **1992**, *188*, 217−222.
(48) Millhauser, G. L.; Freed, J. H. *J. Chem. Phys.* **1984**, *81*, 37−48.
(49) Dzuba, S. A. *Phys. Lett. A* **1996**, *213*, 77−84.
(50) Bartucci, R.; Guzzi, R.; De Zotti, M.; Toniolo, C.; Sportelli, L.; Marsh, D. *Biophys. J.* **2008**, *94*, 2698−2705.
(51) Van, S. P.; Birrell, G. B.; Griffith, O. H. *J. Magn. Reson.* **1974**, *15*, 444−459.
(52) Kulik, L. V.; Salnikov, E. S.; Dzuba, S. A. *Appl. Magn. Reson.* **2005**, *28*, 1−11.
(53) Paschenko, S. V.; Toporov, Yu. V.; Dzuba, S. A.; Tsvetkov, Yu. D.; Vorobiev, A. K. *J. Chem. Phys.* **1999**, *110*, 8150−8154.
(54) Dzuba, S. A. *Spectrochim. Acta, Part A* **2000**, *56*, 227−234.
(55) Isaev, N. P.; Dzuba, S. A. *J. Phys. Chem. B* **2008**, *112*, 13285−13291.
(56) Kirilina, E. P.; Dzuba, S. A.; Maryasov, A. G.; Tsvetkov, Y. D. *Appl. Magn. Reson.* **2001**, *21*, 203−221.
(57) Poluektov, O. G.; Utschig, L. M.; Dalosto, S.; Thumauer, M. C. *J. Phys. Chem. B* **2003**, *107*, 6239−6244.
(58) Parak, F. G.; Achterhold, K.; Schmidt, M.; Prusakov, V.; Croci, S. *J. Non-Cryst. Solids* **2006**, *352*, 4371−4378.
(59) Doster, W *Biochim. Biophys. Acta* **2010**, *1804*, 3−14.
(60) Scarpelli, F.; Bartucci, R.; Sportelli, L.; Guzzi, R. *Eur. Biophys. J.* **2011**, *40*, 273−279.
(61) Curry., S.; Mandelkow., H.; Brick., P.; Franks., N. *Nat. Struct. Biol.* **1998**, *5*, 827−835.